RSC Advances

ROYAL SOCIETY OF CHEMISTRY

www.rsc.org/advances

Banded Spherulites Templated Three-Dimensional Interpenetrated Nanoporous Materials

Lijun Ye, Jishan Qiu, Tao Wu, Xianchun Shi, Yongjin Li*

College of Materials, Chemistry and Chemical Engineering, Hangzhou Normal University, Hangzhou 310036, China

● To whom correspondence should be addressed. Email: yongjin-li@hznu.edu.cn, TEL: 86-571-2886-7206; FAX: 86-571-2886-7899

ABSTRACT: A “banded spherulites templated” strategy has been developed to fabricate 3-D interpenetrated nanoporous polymeric materials. Poly(oxymethylene) (POM) crystallizes into large banded spherulites with incorporation of poly(L-lactic acid) (PLLA) at high temperature. The amorphous PLLA components are simultaneously expelled out from the twisted POM crystal lamellae during the crystallization of the POM components. Therefore, a fully co-continuous phase structure is formed with the interpenetration of POM twisted lamellae and the amorphous PLLA phase. The nanoporous POM materials with high porosity and large specific surface area were successfully obtained after extracting the PLLA phase between the twisted POM lamellae. The 3-D interconnected nanoporous POM films obtained using this strategy could be used in various applications. Moreover, such a strategy should also be applicable to other polymer blend systems and it provides a new route for fabricating nanoporous polymeric materials.

Porous polymeric materials exhibit many attractive properties, such as low density, high specific surface area, high adsorption capacity, uniform and tunable pore sizes. They have been widely used in various applications including gas storage[1-4], adsorption[5,6], separations[7,8], catalysis[9-11], electronic devices[12] and drug delivery[13]. Recently, porous polymeric materials have also been used as growth templates in the synthesis of nanomaterials with specific shapes[14]. Two main strategies have been developed to fabricate porous polymeric materials, i.e., top-down and bottom-up strategies. Johnson and coworkers prepared mesoporous materials using monodisperse silica particles as a template for the first time[15]. The approach is known as "top-down" and introduces templates with ordered structures, e.g. monodisperse SiO_2 particles or anodic aluminum oxide (AAO) templates as sacrificial materials. Alternatively, there is a "bottom-up" path, named the "soft template" approach, by which porous polymeric materials are obtained by etching or dissolving a block segment of block copolymers with a periodically preformed ordered structure via microphase separation. Nakahama's group[16] first fabricated nanoporous polystyrene (PS) membranes via the microphase separation of polystyrene-b-polyisoprene copolymers. The fabrication of nanoporous polymeric materials via microphase separation has attracted a good deal of attention during the last 30 years because of the uniform nanosized pores obtained in these materials.[17-21] Similarly, binary blends of two immiscible polymers A and B at a certain component ratio, sometimes compatibilized with a coupling agent, can self-organize into interpenetrating continuous structures, where each phase is independently continuous in three dimensions. Removal of one of the phases will result in the residue materials forming a 3-D interconnected porous network with an inherently high specific surface area. Favis et al. blended PS with PLLA, in the presence of a PS-b-PLLA copolymer as a compatibilizer, forming interconnecting bicontinuous structures[22-24] On removal of the PS component they obtained 3-D interpenetrating porous PLLA monoliths, which have substantial potential for medical and biological applications. However, there are several disadvantages in adopting such a strategy. On the one hand, the materials usually have micrometer-scale pores because of thermodynamic immiscibility. On the other hand, the co-continuous structure can only be obtained over a very limited component ratio range, and further, porosity of the porous materials is also confined to a very narrow range. Finally, the co-continuous structure from the immiscible blends is usually unstable on thermal annealing or exposure to mechanical shear, and leads to inhomogeneity in the

pore structure.

Banded spherulites are commonly observed in many crystalline polymers, especially in miscible crystalline/amorphous polymer blends. The spherulites exhibit concentric rings or extinction bands in a polarized light microscope (PLM), generally considered arising from the cooperative twisting of radiating lamellar crystals along their fastest growth axis. The accumulation of stress at lamellar surfaces was generally considered the mechanism for lamellar twisting, which has been confirmed during spherulite growth processes using real-time atomic force microscopy (RT-AFM).[25-28] In binary blends, the development of stresses might be controlled mainly by the expulsion of the amorphous components near the fold surfaces during crystallization of the crystalline phase.[29] We consider that the process and formation of the banded spherulites provide a feasible fabrication strategy for obtaining porous polymeric materials. The amorphous components are simultaneously expelled out from the twisted crystal lamellae during the crystallization of the crystalline components. Therefore, a 3-D network forms with interpenetrated crystal lamellae and the amorphous component between the lamellae. Perfect 3-D porous materials can be obtained simply by removing the amorphous material lying between the twisted lamellae. In this work, we have, for the first time, succeeded in fabricating highly ordered POM nanoporous materials by selectively etching the PLLA phase from the banded POM spherulites in the PLLA/POM blends.

We have made systematic investigations into the phase behavior of binary PLLA/POM blends using small-angle light scattering (SALS) and optical microscopy. It was found that PLLA/POM exhibited typical low critical solution temperature (LCST) phase behavior. PLLA and POM are fully miscible in the melt state at low temperature because of the weak interaction between the CH_2 groups of POM and the CO groups of PLLA.[30] Although both POM and PLLA are crystalline polymers, the crystallization rate of POM is much higher than that of PLLA, as confirmed by DSC cooling curves of the PLLA/POM blends from the melt state. No exothermic peak for neat PLLA sample was observed at the cooling rate of 10 ^{o}C/min from the melt (Figure 1(a)). Moreover, two crystal diffraction peaks at 2θ =22.7 and 34.8 ^{o} in the WAXD pattern (Figure 1(b)) were observed for the all POM/PLLA blends, same to those for the neat POM. The two diffraction peaks corresponds to the (100) and (105) peaks of POM hexagonal crystals, respectively. [31] The fact that POM/PLLA blends have the same crystal form as the neat POM

indicates that PLLA molecular chains are expelled out from the POM crystal lamellae and no co-crystallization occurs in the blends. At the same time, no PLLA crystal diffraction peaks were observed in the blends, indicating the PLLA are in amorphous state in the blends at the crystallization conditions presented here. Therefore, the amorphous PLLA molecular chains are located between the POM lamellae (or stacks) to form an interlamellar structure. POM has even higher crystallinity (as high as 80%, see Table 1) in the blends than in the neat POM. High POM crystallinity implies that few amorphous POM chains are mixed with PLLA located in the POM interlamellar region. The addition of PLLA decreases the equilibrium melting points of POM, so the supercooling is smaller for the blends than for the neat POM at the same crystallization temperature. Therefore, the larger spherulites and slightly increased crystallinity can be expected for the blends.

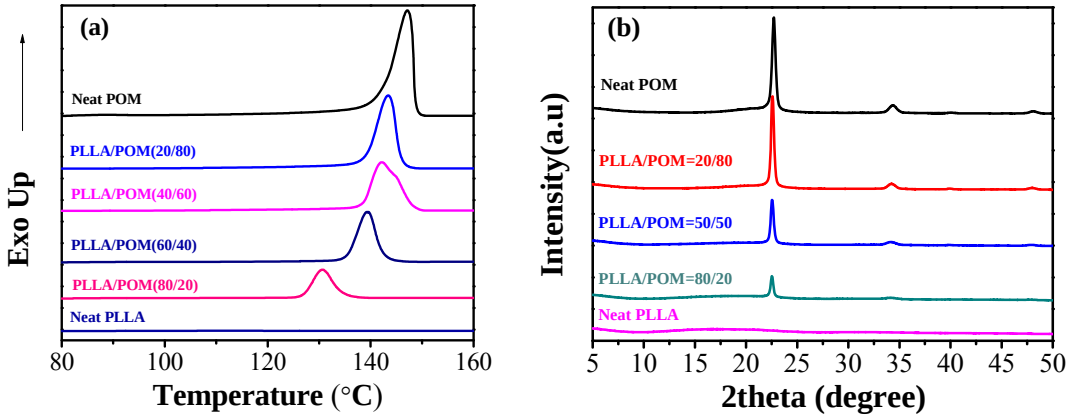

Figure 1. (a) DSC curves of cooling scans at 10 ^{o}C/min for Neat POM and PLLA/POM blends, and (b) Wide-angle X-ray diffraction curves of PLLA/POM blends.

Table 1 POM crystallinity from DSC in neat POM and PLLA/POM blends crystallized at 141^{o}C for 0.5 hours followed by quenching to room temperature

PLLA/POM	0/100	20/80	40/60	60/40	80/20
X_c of POM	76.9 %	79.7 %	80.1 %	85.5 %	88.4 %

Figure 2 shows the polarized optical images of isothermally crystallized PLLA/POM blend films with the indicated compositions. All the samples were prepared first by hot pressing at 190

°C followed by rapid cooling to 141 °C to allow the isothermal crystallization of POM. After complete crystallization of POM for 0.5 h, the sample was rapidly quenched to room temperature. During this processing, POM in the blends was fully crystallized because of the high crystallization rate, while all the PLLA molecular chains within the blends were maintained in the amorphous state because of the relatively slow crystallization rate. This was evident by the WAXD pattern of the sample, which showed the diffraction peaks of POM alone (Figure 1(b)). It is clear that the neat POM crystallized into the common spherulites, while neat PLLA could not crystallize at the presented conditions. In contrast, the incorporation of PLLA into POM spherulites leads to the extremely regular and large POM banded textures. Such phenomena have been observed for many miscible crystalline/amorphous polymer blends [32-34]. It is generally accepted that lamellae show twisting behavior along the radial direction with the phase angle of twist coherent along the tangential direction in banded spherulites.[35] Such lamellar twisting originates from the unbalanced surface stresses caused by the steric hindrance of chain folding on the folding surfaces.[36] POM and PLLA are miscible in the melt state. It is therefore considered that the PLLA molecules were selectively adsorbed on the folding surfaces of the POM lamellar crystallites (involving weak interactions between them) and thereby cause surface stresses, resulting in the twisting phenomena. At the same time, the expulsion of PLLA from the POM crystal lamellae leads to additional surface stresses and thereby enhances such twisting. Therefore, POM-banded spherulites for the blends were obtained.

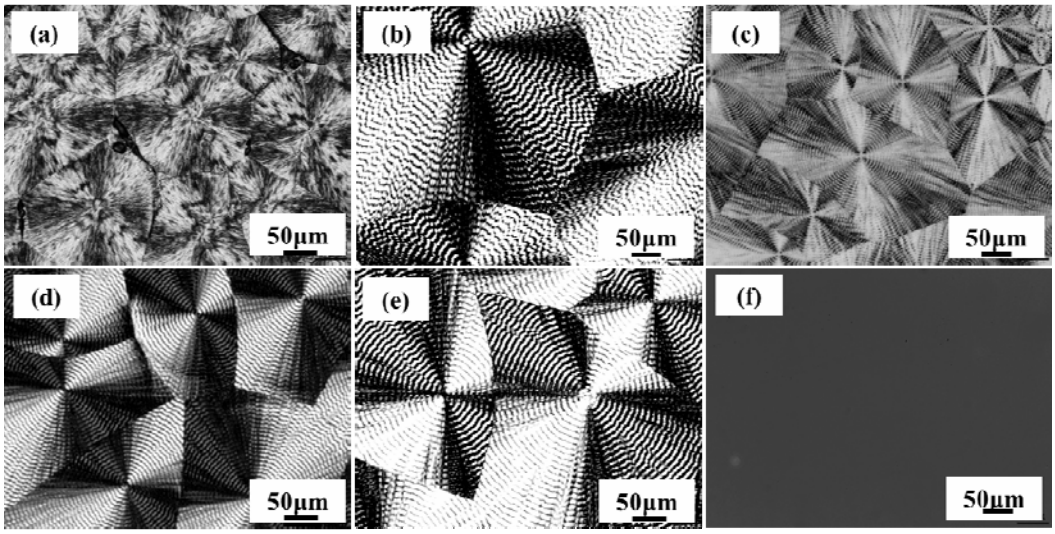

Figure 2. The polarized optical images of PLLA/POM blends. (a) Neat POM, (b) PLLA/POM=40/60, (c) PLLA/POM=50/50, (d) PLLA/POM=60/40, (e) PLLA/POM=80/20, and (f) Neat PLLA.

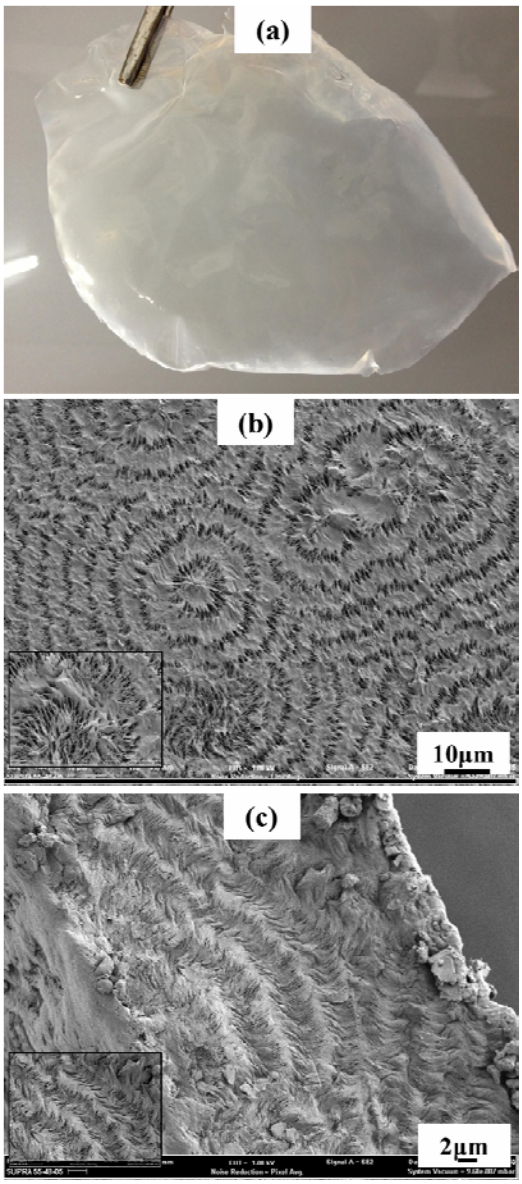

Figure 3. (a) The self-supporting film of PLLA/POM (50/50) after etching of PLLA, (b) SEM image of the film surface of crystallized PLLA/POM (50/50) sample after etching, and (c) SEM image of the fracture surface (fractured on the film thickness direction) of crystallized PLLA/POM (50/50) after etching.

We consider that the POM-banded spherulites are a good template for fabricating interconnected nanoporous materials. PLLA/POM blends form a co-continuous structure with POM twisted lamellae and an amorphous PLLA phase between the POM lamellae during high-temperature isothermal crystallization. Therefore, POM porous materials can be obtained by simple extraction of the PLLA phase. Chloroform is a good solvent for PLLA and a non-solvent

for POM. Figure 3(a) shows the microscopic image of PLLA/POM (50/50) blend film after solvent etching by chloroform. It is clear that the film after extraction not only maintains the original shape, but is also translucent and very tough. A gravimetric method was used to calculate the extent of continuity of the POM phase. It was calculated that all the PLLA was extracted (close to 100 %). Moreover, it was further found that the extracted solution contains only PLLA and the film after the extraction comprised neat POM (as evidenced by the FTIR measurements in Figure S1). This indicates again the fully extraction of PLLA and the fabrication of interconnected POM channels. Figure 3(b) and (c) show the SEM images of the film surface and fracture surface, respectively, after the extraction of PLLA. It is found that the sample after PLLA extraction maintained the POM banded spherulites texture (Figure 2(c)), but numerous pores are found. Moreover, the pores exhibit periodicity, identical to that found with the banded spherulites. Figure 3(c) shows the SEM of the fracture surface of the extracted sample, and shows the internal pore structure of the extracted film. It is obvious that all the pores are interconnected to form a 3-D network, so that all the PLLA can be fully extracted by simple solvent etching. For the lamellae of POM spherulites (Figure 3(b), (c)), helical growth took place from the center and slightly wavy lamellar morphologies were seen. We speculate that the wavy morphologies might be a typical characteristic of lamellar twisting, similar to that previously reported by Ho and coworkers.[37,38] Therefore, after etching of amorphous PLLA chains, highly ordered and periodic rings that consisted of numerous nanoscale interpenetrating pores were observed in the surface and fracture surfaces of the PLLA/POM (50/50) blend. These results are consistent with the PLM data described above.

It is very interesting to find that a 3-D interconnected porous film can be achieved by simple solvent etching of the crystallized PLLA/POM blends. The surfaces and fractures of all the etched PLLA/POM samples exhibited high-porosity microstructures and the structure of the porous film is very similar to that of the banded spherulite of the blend before extraction. We therefore undertook a detailed analysis of the formation of such novel nanoporous structures. Figure 4(a) and (b) show the surface topography of a banded spherulite in the PLLA/POM (50/50) sample before and after solvent etching, as observed with atomic force microscopy (AFM). Highly ordered and periodically banded “peaks and valleys” (due to the formation of an alternative flat-on and edge-on lamellar morphology) could be seen along the growth axis of the POM spherulites.

The periodicity of the topographic variation was in good agreement with the pitch length of the extinctions that were observed in PLM. We suggest that the POM lamellae were arrayed perpendicular to the observation plane to form the "peaks" while those parallel to the plane would produce the "valleys" (Figure S2). The height difference between peaks and valleys is about 70 nm, as revealed by cross-section analysis (Figure 4(a)). However, this difference increases to about 450 nm after solvent etching. This indicates that the etched amorphous PLLA had initially aggregated and filled the volume of these valleys, to form a highly continuous phase. In other words, in the presence of amorphous PLLA, the lamellae of POM twisted to form an assembly of banded spherulites, resulting in the volume-filling of PLLA in the interlamellar regimes and the self-templating of the formation of a 3-D interpenetrating nanoporous network via etching of amorphous PLLA. The pore formation mechanism is summarized as shown in Figure 4(c). Under isothermal crystallization conditions, POM lamellae form and grow in the presence of amorphous PLLA from the homogenous PLLA/POM blend melt. They cooperatively twist along their fastest growth axis because of the stress accumulation and finally they assemble into banded spherulites. During crystallization of POM, as presented in Figure 4(c), the amorphous PLLA chains were gradually expelled out from the homogenous mixture of PLLA and POM (microphase separation), and became located in the interlamellar regimes, because of their favorable-interactions with the POM amorphous chains. The component phases consequently interpenetrated to form a continuous amorphous phase. That is, upon the crystallization of POM, POM and PLLA independently and synchronously formed continuous phases, and the final result was the construction of a highly interpenetrated network (co-continuous structure). As a consequence, the 3-D interpenetrated nanoporous POM materials, after removal of the continuous amorphous PLLA phases, could easily be achieved.

Obviously, the pore structure is only dependent upon the spherulites structure of the blends, according to the pore formation mechanism in Figure 4. We therefore investigated the influence of the crystallization conditions and the compositions of the blends on the pore structure after extracting (as shown in Figures S3 and S4, respectively). Although no well-developed POM spherulites were obtained for the quenched PLLA/POM (50/50) blends, the porous films with high porosity can still be achieved (Figure S3). On the other hand, we found that the PLLA/POM blends with the compositions ranging from 80/20 to 20/80 can be used to prepare porous POM

materials, but with various pore structures (Figure S4). High content of PLLA leads to enhanced porosity of the final porous POM films due to the low POM volume fraction. Therefore, the schematic diagram in Figure 4 is also applicable for all blend compositions of the presented blend. The detail manipulation of the pore structure by adjusting crystallization conditions and component ratios is under investigation and will be reported in the near future.

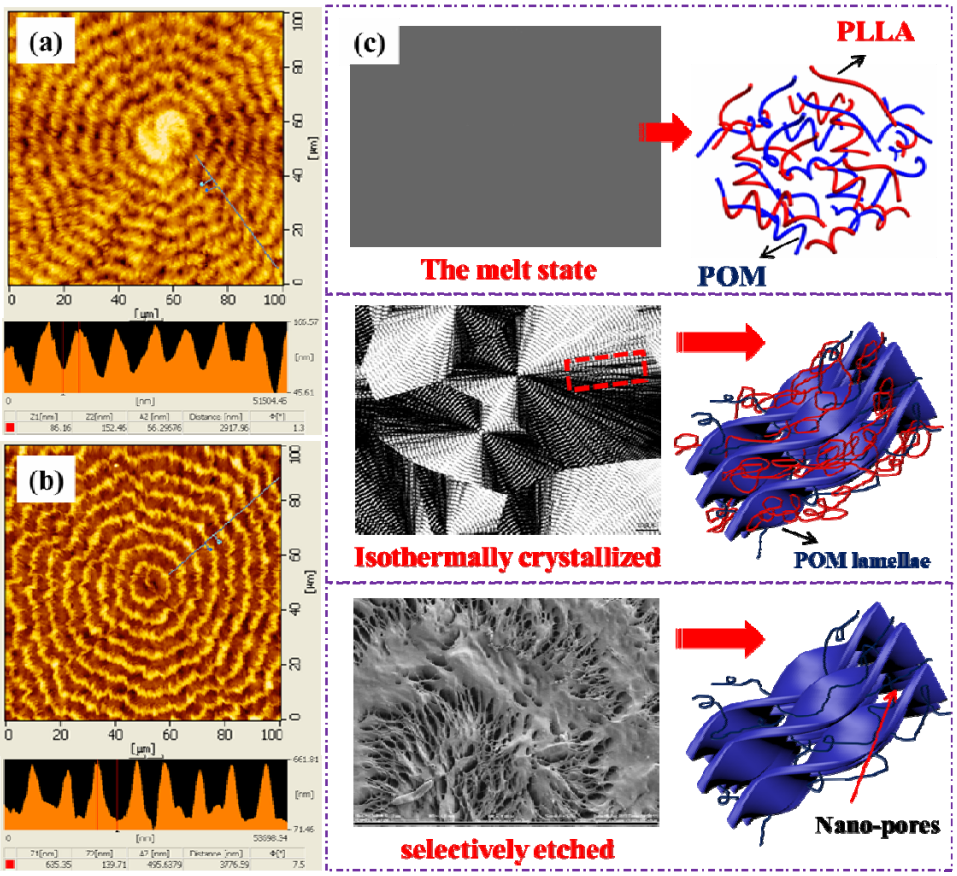

Figure 4. (a) AFM images (topography) of a POM banded spherulite from PLLA/POM (50/50) blend, (b) AFM image showing (topography) after etching, and (c) Schematic illustration of the "banded spherulite templated" path to fabricate the 3-D nanoporous POM materials.

To further verify the construction of a 3-D interpenetrating network, the thin films, after etching, have been used for filtration tests and water flux measurements. It was found that the film could be used as a filtration "paper" and water can flow continuously through the filtration equipment (Video S1). This again indicates the 3-D interconnected porous structure of the film. The porous film from the isothermally crystallized 50/50 blend shows a water flow of more than 30 L/m^2h by the water flux test under 0.3MPa (Figure 5(a)). This value is fairly large and suggests

a potential application as a water purification film. Both BET and mercury intrusion methods have been used to accurately evaluate the pore size and porosity. As shown in Figure 5 (b), the average pore size is almost same for the porous films from the well crystallized PLLA/POM (50/50) and PLLA/POM (60/40) blends. However, the crystallization condition shows drastic influence on the pore size of the porous sample. The films from the isothermally crystallized samples have the pore sizes that are several ten nanometers larger than those from the quenched samples (ca. 18 nm). This can be attributed to the larger interlamellar distance for the isothermally crystallized sample. The porosity and the specific surface area of the porous film from isothermally crystallized 50/50 sample are as large as 80% and 48.1 m^2/g, respectively. Note that the pore size by BET and mercury measurements is much smaller than the size directly observed from SEM images (about 0.5-1μm). Such differences can be attributed to the overlapping of the pores in the direction of the film thickness. Further, the porous film from the isothermally crystallized PLLA/POM (50/50) containing water shows about 110% elongation at the break and the tensile strength of about 11 MPa, while the quenched one exhibited only about 25% elongation at the break but slight higher tensile strength (as shown in Figure 5 (c)). The mechanical properties of the film are adequate for real (industrial) applications, such as the water filtration under pressure.

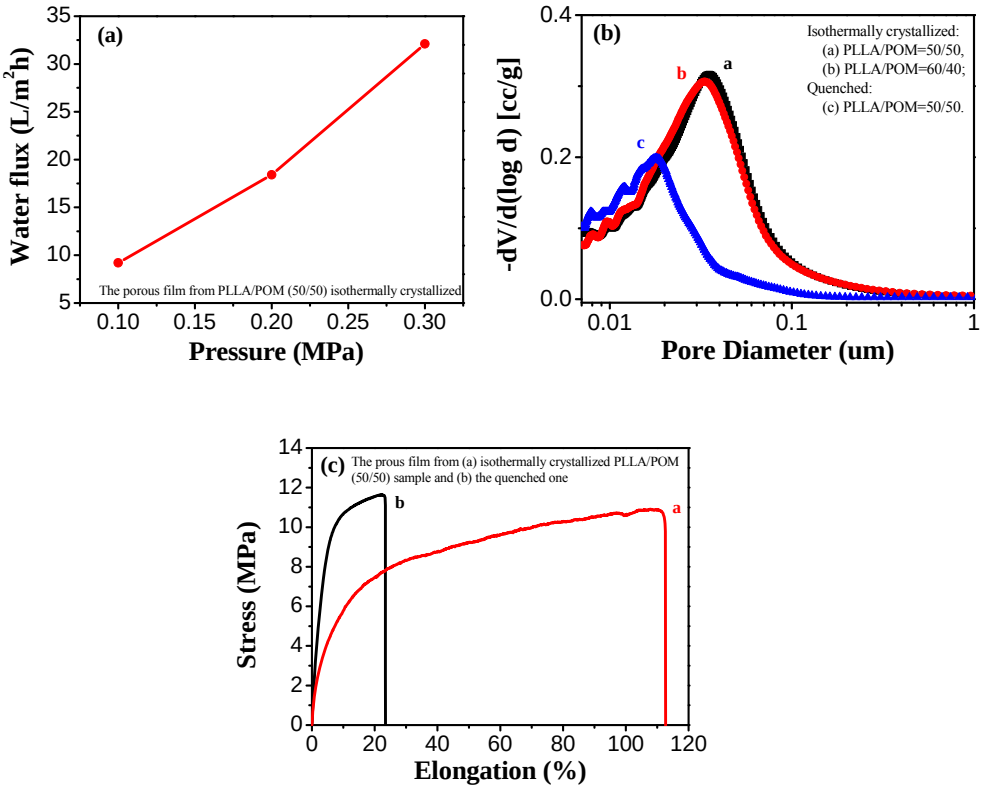

Figure 5. (a) Water flux of porous POM as a function of the pressure, (b) pore size distribution porous POM (after removal of PLLA), and (c) strain-stress curves of the POM nanoporous films containing water for water flux measurements.

In conclusion, a simple, sensible and accessible route to the successful fabrication of nanoporous polymeric materials was demonstrated. Crystallization-induced microphase separation occurred during the crystallization of POM from the homogenous PLLA/POM melts. The PLLA was expelled out from the twisted POM lamellar crystals and porosity developed upon extraction of the PLLA. The porous POM films exhibit high porosity and a mean pore size of several tens of nanometers. The pore size, porosity and specific surface area can be manipulated by varying the blend compositions and crystallization conditions. It is expected that such 3-D interconnected nanoporous materials can be used in various applications. Moreover, such a synthetic strategy should be applicable to other polymer blend systems and it therefore offers a new route for obtaining nanoporous polymeric materials.

This work was financially supported by the National Science Foundation of China (51173036, 21374027) and the Ministry of education program for New Century Excellent Talents, and PCSIRT (IRT 1231).

Notes and references

College of Materials, Chemistry and Chemical Engineering, Hangzhou Normal University, Hangzhou, 310036, P. R. China. FAX: +86 571 28867899; Telephone: +86 571 28867026; E-mail: Yongjin-li@hznu.edu.cn.

† Electronic Supplementary Information (ESI) available: Experimental details, Figs. S1, S2, S3, and S4 and video S1. See DOI: 10.1039/b000000x/

1 P. M. Budd, A. Butler, J. Selbie, K. Mahmood, N. B. McKeown, B. Ghanem, K. Msayib, D. Book, A. Walton, *Phys Chem Chem Phys*. 2007, **9**, 1802.

2 N. B. McKeown, P. M. Budd, D. Book, *Macromol. Rapid. Commun.* 2007, **28**, 995.

3 F. Svec, J. Germain, J. M. J. Fréchet, *Small* 2009, **5**, 1098.

4 R. E. Morris, P. S. Wheatley, *Angew. Chem. Int. Ed*. 2008, **47**, 4966.

5 J. E. G. J. Wijndhoven, W. L. Vos, *Science*. 1998, **281**, 802.

6 B. T. HollandT, C.E. Blandford, A. Stein, *Science*. 1998, **281**, 538.

7 A. A. Zakhidov, R. H. Baughman, Z. Lqbal, *Science*. 1998, **282**, 897.

8 Y. A. Vlasov, N. Yao, D. J. Norris, *Adv. Mater.* 1999, **11**, 165.

9 Y. H. Guo, C. W. Hu, X. L. Wang, Y. H. Wang, E. B. Wang, Y. C. Zou, H. Ding, S. H. Feng, *Chem. Mater*. 2001, **13**, 4058.

10 A. Bolognesi, C. Mercogliano, S. Yunus, M. Civardi, D. Comoretto, A. Turturro, *Langmuir*. 2005, **21**, 3480.

11 J. Y. Ying, *AIChE J*. 2000, **46**, 1902.

12 N. Haberkorn, M. C. Lechmann, B. H. Sohn, K. Char, J. S. Gutmann, P. Theato, *Macromol. Rapid Commun*. 2009, **30,** 1146.

13 E. A. Jackson, M. A. Hillmyer, *ACS Nano.* 2010, **4**, 3548.

14 M. J. Xue, W. T. Xiao, Z. J. Zhang, *Adv. Mater*. 2008, **20**, 439.

15 S. A. Johnson, P. J. Ollivier, T. E. Mallouk, *Science*. 1999, **283**, 963.

16 J. S. Lee, A. Hirao, S. Nakahama, *Macromolecules*. 1988, **21**, 274.

17 U. Jeong, D. Y. Ryu, J. K. Kim, D. H. Kim, T. P. Russell, C. J. Hawker, *Adv. Mater.* 2003, **15**, 1247.

18 A. S. Zalusky, R. Olayo-Valles, J. H. Wolf, M. A. Hillmyer, *J. Am. Chem. Soc*. 2002, **124**,

12761.

19 J. Rzayev, M. A. Hillmyer, *J. Am. Chem. Soc.* 2005, **127**, 13373.

20 R. M. Ho, Y. W. Chiang, C. K. Chen, H. W. Wang, H. Hasegawa, S. Akasaka, E. L. Thomas, C. Burger, B. S. Hsiao, *J. Am. Chem. Soc*. 2009, **131**, 18533.

21 H. Zhao, W. Gu, R. Kakuchi, Z. W. Sun, E. Sterner, T. P. Russell, E. B. Coughlin, P. Theato, *ACS Maco. lett*. 2013, **2**, 966.

22 P. Sarazin, B. D. Favis, *Biomacromolecules.* 2003, **4**, 1669.

23 P. Salehi, P. Sarazin, B. D. Favis, *Biomacromolecules.* 2008, **9**, 1131.

24 Z. Y. Xiang, P. Sarazin, B. D. Favis, *Biomacromolecules.* 2009, **10**, 2053.

25 A. J. Owen, *Polymer*. 1997, **38**, 3705.

26 H. D. Keith, F. J., Jr. Padden, *Polymer.* 1984, **25**, 28.

27 A. Keller, *J Polym Sci*. 1955, **17**, 291.

28 H. D. Keith, F. J., Jr. Padden, B. Lotz, J. C. Wittman, *Macromolecules.* 1989, **22**, 2230.

29 J. P. Liu, B.-J. Jungnickel, *J. Polym. Sci: Part B: Polym. Phys.* 2007, **45**, 1917

30 J. S. Qiu, C. Y. Xing, X. J. Cao, H. T. Wang, L. Wang, L. P. Zhao, Y. J. Li, *Macromolecules*, 2013, **46**, 5806.

31 J. S. Qiu, J. P. Guan, H. T. Wang, S. Zhu, X. Cao, Q. L. Ye, Y. J. Li. *J. Phys. Chem. B*, 2014, **118,** 7167.

32 H. D. Keith, F. J., Jr. Padden, T. P. Russell, *Macromolecules*. 1989, **22**, 666.

33 W. Li, R. Yan, B. Jiang, *Polymer*, 1992, **33**, 889.

34 A. Toda, K. Taguchi, H. Kajioka, *Polymer*, 2002, **53**, 1765.

35 T. Ikehara, H. Jinnai, T. Kaneko, H. Nishioka, T. Nishi, *J. Polym. Sci. B Polym. Phys.* 2007, **45**, 1122.

36 B. Lotz, S. Z. D. Cheng, *Polymer* 2005, **46**, 577.

37 R. M. Ho, K. Z. Ke, M. Chen, *Macromolecules*, 2000, **33**, 7529.

38 C. C. Chao, C. K. Chen, Y. W. Chiang, R. M. Ho, *Macromolecules*, 2008, **41**, 3949.